









# Resolving Interchange Reconnection Dynamics in a Fan-Spine-like Topology Observed by Solar Orbiter

Yadan Duan <sup>1,2,3\*</sup>, Xiaoli Yan <sup>1,2</sup>, Junchao Hong <sup>1</sup>, Hechao Chen <sup>2,4</sup>, Yuhang Gao <sup>3,5</sup>, Zheng Sun <sup>3,6</sup>,  
Zhenyong Hou <sup>3</sup>, and Jincheng Wang <sup>1,2</sup>

<sup>1</sup> Yunnan Observatories, Chinese Academy of Sciences, Kunming, 650216, China  
e-mail: duanyadan@ynao.ac.cn

<sup>2</sup> Yunnan Key Laboratory of Solar Physics and Space Science, Kunming, 650216, People's Republic of China

<sup>3</sup> School of Earth and Space Sciences, Peking University, Beijing, 100871, People's Republic of China

<sup>4</sup> School of Physics and Astronomy, Yunnan University, Kunming, 650500, China

<sup>5</sup> Centre for Mathematical Plasma Astrophysics, Department of Mathematics, KU Leuven, Celestijnenlaan 200B bus 2400, B-3001 Leuven, Belgium

<sup>6</sup> Leibniz Institute for Astrophysics Potsdam, An der Sternwarte 16, Potsdam 14482, Germany

Submit

## ABSTRACT

Interchange reconnection is believed to play a significant role in the production of solar jets and solar wind. However, the dynamics of interchange reconnection in the low corona might be more complex than recognized before in higher temporal and spatial resolutions. Using unprecedentedly high-resolution observations from the Extreme Ultraviolet Imager (EUI) onboard the Solar Orbiter, we analyze the dynamics of interchange reconnection in a small-scale fan-spine-like topology. Interchange reconnection that continuously occurs around the multi-null points of the fan-spine-like system exhibits a quasi-periodicity of  $\sim 200$  s, nearly covering the entire evolution of this system. Continuous evolution and reversal of multiple current sheets are observed over time near the null point. These results reveal that the dynamics of interchange reconnection are likely modulated by the emerging magnetic structures, such as mini-filaments and emerging arcades. Moreover, a curtain-like feature with a width of 1.7 Mm is also observed near the interchange reconnection region and persistently generates outflows, which is similar to the separatrix curtain reported in the pseudo-streamer structure. This study not only demonstrates the complex and variable reconnection dynamics of interchange reconnection within small-scale fan-spine topology but also provides insights into the self-similarity of magnetic field configurations across multiple temporal and spatial scales.

**Key words.** Sun: activity – Sun: corona – Sun: magnetic topology – magnetic reconnection

## 1. Introduction

Interchange reconnection represents a fundamental physical process in the solar atmosphere. It is characterized by the reconnection between closed magnetic field lines and adjacent open magnetic fields of opposite polarity (Fisk et al. 1998; Crooker et al. 2002). It can lead to a rapid conversion of magnetic energy, enabling the transfer of mass and energy along magnetic field lines. Meanwhile, interchange reconnection can cause plasma heating and particle acceleration, allowing energetic electrons to escape into interplanetary space along open magnetic field lines. Additionally, interchange reconnection is also an effective way to release the magnetic twist from closed magnetic fields into the interplanetary space environment (e.g., Bale et al. 2019; Sterling & Moore 2020; Sterling et al. 2020). In the solar corona, diverse magnetic field configurations are conducive to the occurrence of interchange reconnection. Therefore, characterizing interchange reconnection dynamics in different magnetic field configurations is crucial for the triggering mechanisms for solar jets (e.g., Shibata et al. 1992; Krucker et al. 2011), as well as understand the origin and properties of the solar wind (e.g., Masson et al. 2014; Pellegrin-Frachon et al. 2023).

Pseudo-streamers, as one of the large-scale coronal structures, provide a favorable environment for the occurrence of interchange reconnection. Pseudo-streamer separates open field lines of the same polarity and contains two closed magnetic flux below its cusp (Wang et al. 2007), displaying a  $\mathfrak{H}$ -type structure. The pseudo-streamers are usually located more than 1.5 solar radii above the solar surface and are formed by multiple null points linked by separators (e.g., Titov et al. 2011, 2012; Seaton et al. 2013; Masson et al. 2014). In such a configuration, a strong gradient of magnetic connectivity exists among open and closed magnetic fields (e.g., Masson et al. 2014; Scott et al. 2021; Pellegrin-Frachon et al. 2023), known as Separatrix-Web (S-Web) and predicted to favor the occurrence of interchange reconnection. The S-Web model was proposed by Antiochos et al. (2011), Titov et al. (2011), and Linker et al. (2011), showing a network of separatrix surfaces and quasi-separatrix layers (QSLs). Simulation studies demonstrate that a vertical fan surface emanates from the null points, referred to as a separatrix curtain, which exhibits a curtain-like shape (e.g., Masson et al. 2014; Scott et al. 2021; Pontin & Priest 2022). The separatrix curtain is surrounded by QSLs, which results from a rapid divergence of the field lines in the vicinity of the null points associated with the separatrix surfaces (Titov et al. 2011). The interchange reconnection occurring in pseudo-streamers is a gradual physical

\* Corresponding author; duanyadan@ynao.ac.cn

process (Masson et al. 2014) that can last for several hours without any drastic changes (e.g., Seaton et al. 2013). The pseudo-streamer topology, which may more accurately reflect the actual magnetic structure of the system, is thought to play a significant role in the generation of the slow solar wind. Therefore, understanding the dynamics of this system is crucial for analyzing the mass and energy release of the slow solar wind. Recently, Chitta et al. (2023) utilized middle coronal observations to investigate the dynamics of pseudo-streamer systems, providing observational evidence that the reconnection dynamics along the S-Web are responsible for the release of slow solar wind plasma. However, observing such a dynamic process of the pseudo-streamer system in high coronal still remains challenging.

The fan-spine structure is defined by a dome-shaped fan separatrix surface, a magnetic null point positioned at its apex, and the inner and outer spines passing through the null point (e.g., Priest & Forbes 2002; Li et al. 2021; Pontin & Priest 2022). Similar to the large-scale pseudo-streamers, a smaller-scale fan-spine structure is also a desirable place for the occurrence of interchange reconnection. Recent observations revealed that the magnetic null point position of fan-spine configurations is approximately 1–6 Mm above the solar surface (e.g., Cheng et al. 2023; Duan et al. 2024b). The fan-spine topology is thus associated with various small-scale solar phenomena, such as solar jets (e.g., Liu et al. 2011; Wang & Liu 2012; Hong et al. 2017; Shen et al. 2019; Duan et al. 2022), solar flares (e.g., Sun et al. 2013; Li et al. 2018; Song & Tian 2018; Zhong et al. 2019; Yang et al. 2020b), ultraviolet bursts (e.g., Chitta et al. 2017; Chen et al. 2019b; Bhatnagar et al. 2025b), Ellerman bombs (e.g., Bhatnagar et al. 2025a), macropicules (e.g., Duan et al. 2023), small-scale spiral jets (e.g., Cheng et al. 2023; Li et al. 2025b), jetlets (e.g., Kumar et al. 2022; Yang et al. 2025), and coronal bright points (e.g., Zhang et al. 2012; Færder et al. 2024; Nóbrega-Siverio et al. 2025). Currently, an increasing number of observations and simulations support that jets and flares could result from magnetic reconnection between the magnetic flux rope (or filament) initially confined below the fan and the magnetic field of the outer fan (e.g., Jiang et al. 2013; Song et al. 2018; Wyper et al. 2017, 2018; Yang et al. 2020a; Zhou et al. 2021; Duan et al. 2024b; Yang et al. 2024a). After the eruption, the remains of an inner bright patch encircled by a circular flare ribbon can be observed on the solar surface (e.g., Masson et al. 2009; Liu et al. 2015; Hou et al. 2019; Ning et al. 2022; Zhang 2024), and these features indicate the footpoint positions of the inner spine and the dome-like fan separatrix surface, respectively. The lifetime of circular ribbon flares ranges from 4 to 205 minutes, with a mean value of approximately 50 minutes (Zhang et al. 2022). The speeds and ejection heights of solar jets can reach several hundred kilometers per second and several hundred Mm, respectively.

Interchange reconnection around the null point in the fan-spine system is also an active field of theoretical and numerical research, which aids in understanding the transfer of magnetic flux across different topological regions (e.g., Pariat et al. 2009; Masson et al. 2012; Fuentes-Fernández & Parnell 2013; Pontin et al. 2013; Pontin & Priest 2022). Traditional studies have generally considered that fan-spine structures contain a single null point (e.g., Pariat et al. 2009; Wyper et al. 2017), which differs from pseudo-streamer structures that are formed by several null points linked by separators (e.g., Titov et al. 2012). However, research by Duan et al. (2024b) reported that fan-spine topology may contain more than one null point (potentially multiple null points, or QSLs, or separators). Duan et al. (2024b) found that the position of a current sheet is along the QSL connecting

two null points. Moreover, the small-scale evolving jets can also exhibit various dynamic processes at their base, such as multiple small-scale eruptions, plasma flows, and moving blobs (e.g., Mandal et al. 2022; Long et al. 2023). Thus, the dynamics of interchange reconnection within small-scale fan-spine structures may exhibit more complex reconnection behaviors, necessitating further investigations with higher resolution.

In this paper, we utilize high temporal and spatial resolution data acquired by the Extreme Ultraviolet Imager (EUI; Rochus et al. (2020)) on the Solar Orbiter (SO; Müller et al. (2020)) to investigate the dynamics of interchange reconnection that continuously occurs around the null point of a fan-spine-like structure. Moreover, we also identify a curtain-like feature similar to the large-scale pseudo-streamer within a small-scale fan-spine-like structure.

## 2. Observations

On 2024 April 5, Solar Orbiter (SO) was positioned approximately 0.29 AU from the Sun, at an angle of 83 degrees between SO and Earth relative to the Sun (e.g., Tan et al. 2025). The event of interest occurred at the western limb of the Sun as observed by SO, rendering it completely invisible from Earth. Consequently, all data utilized in this study were obtained from SO. The Extreme Ultraviolet Imager (EUI) aboard SO consists of three telescopes: the Full Sun Imager (FSI) and two High-Resolution Imagers ( $\text{HRI}_{\text{EUV}}$  and  $\text{HRI}_{\text{Ly}\alpha}$ ).  $\text{HRI}_{\text{EUV}}$  174 Å images provide the dynamic evolution of the fan-spine-like structure and the complex interchange reconnection process around the null point within the fan-spine-like system. The  $\text{HRI}_{\text{EUV}}$  174 Å observations feature a time cadence of 16 s, and a pixel scale of 0.''49, with an effective exposure time of 2 s. A pixel corresponds to  $0.108 \times 0.108 \text{ Mm}^2$  on the Sun. The imaging observations in two channels (FSI 174 Å and FSI 304 Å) from the FSI also enable us to study the plasma motions from a larger field of view. The temporal cadence and spatial pixel scale of FSI data are 10 minutes and 4.4'', respectively. We used cross-correlation for data alignment and jitter elimination.

## 3. Results

Figure 1 (a) and (b) present an overview of a fan-spine-like structure observed at the solar limb from the perspective of Solar Orbiter. A closer view of this structure, indicated by the cyan box in Figure 1 (b), is shown in Figure 1 (c) after a 115° counter-clockwise rotation to achieve an upright orientation. Figure 1 (c) reveals that the scale of the fan dome is approximately 15 Mm at the solar limb. At this time, plasma outflows along the outer spine of the fan-spine system display the morphology of an anemone solar jet, characterized by an inverted-Y shape comprising a bright, straight jet spine and a jet base. This inverted-Y feature is thought to be the consequence of reconnection between small-scale magnetic arcades and the unipolar background fields (e.g., Tian et al. 2014a, 2018; Tang et al. 2025). Given the location of this structure at the solar limb and the associated projection effects, we did not use PHI (Solanki et al. 2020) for magnetic field extrapolation (e.g., Petrova et al. 2024) to obtain the fan-spine feature. However, in the context of magnetic reconnection in three-dimensional geometries, the simplest anticipated outcome of flux emergence into a locally unipolar region is the formation of a fan-spine magnetic field configuration (e.g., Török et al. 2009). Thus, the fan-spine topology can represent

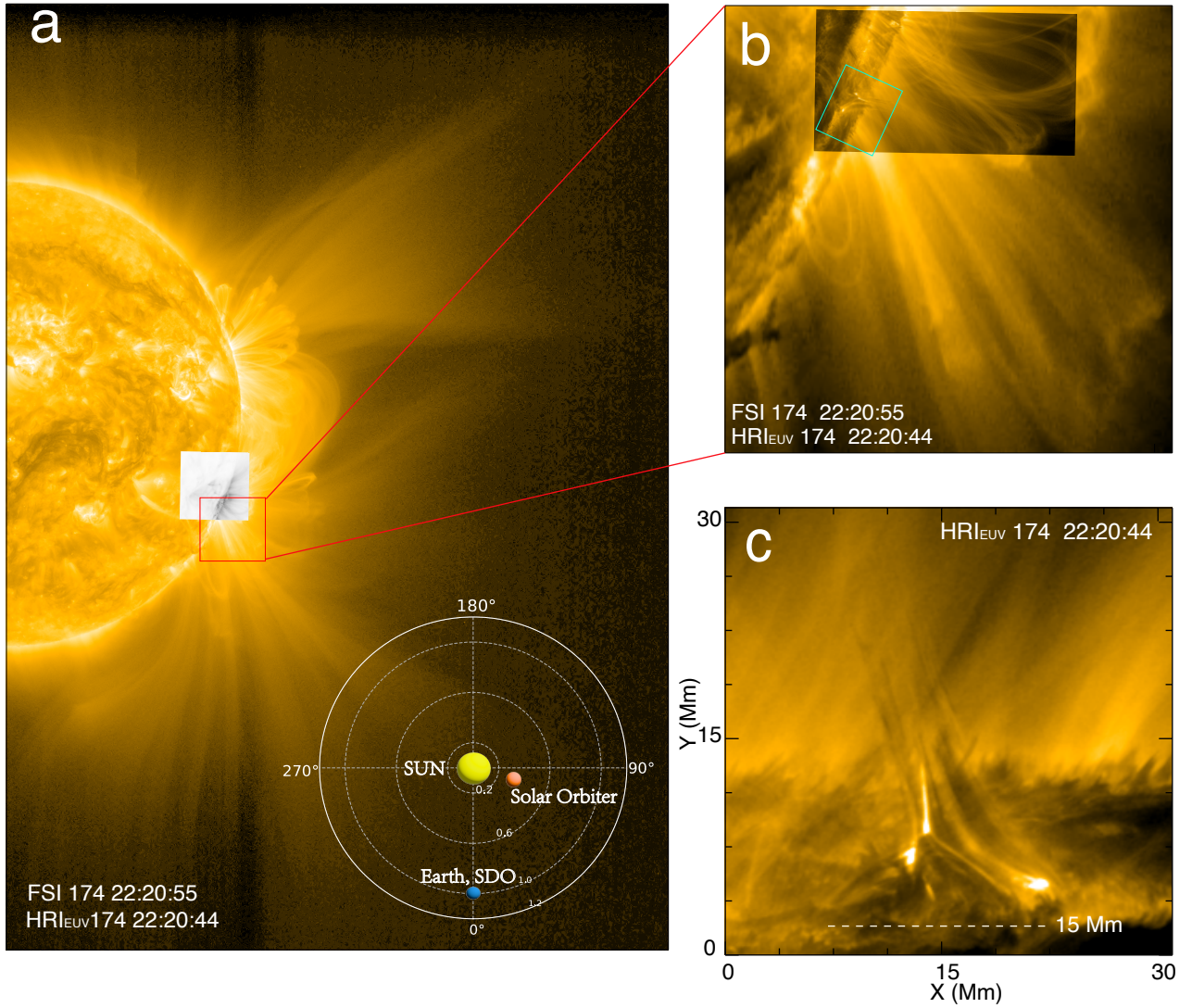


**Fig. 1.** **a:** positions of Solar Orbiter and Earth at 22:20 UT on 2024 April 5; the HRI<sub>EUV</sub> inverted greyscale is overlaid on the FSI<sub>174</sub> image, showing the location of a fan-spine-like structure at this time. The field of view in panel (b) corresponds to the red box indicated in panel (a), showing the HRI overlaid on the FSI image at 22:20 UT **c:** Zoom in of HRI<sub>EUV</sub> 174 Å (cyan box in **b**) showing the structure at the solar limb at a scale of about 15 Mm.

the 3D magnetic structure of the straight anemone jet (e.g., Shen 2021).

Figure 2 exhibits the evolution of the fan-spine-like topology, as observed in HRI<sub>EUV</sub> 174 Å images. At approximately 22:00:44 UT, a small, dark, closed-loop system emerges to the right of the coronal plume region. This dark loop could represent an arch filament system carrying cool material (e.g., Bruzek 1967; Chen et al. 2018; Su et al. 2018). By 22:09:48 UT, the emerged loop gradually expands toward the background coronal loop region. The speed at which the magnetic loop carrying cold material approached the background field is approximately  $2 \text{ km s}^{-1}$ , as shown in Figure 2 (f). At 22:13:48 UT, an X-point, the signal of interaction reconnection between two systems at the reconnection site, is marked by the yellow arrows. This interaction results in the formation of a new closed loop (denoted by the white arrow), as shown in Figure 2 (d). Afterward, a weak sheet-like feature develops near the X-point, connecting the new loop and the open field, as denoted by the cyan arrow in Figure

2 (d). Such a sheet-like structure delineates the current sheet associated with the reconnection configuration, as suggested by previous observational studies (e.g., Tian et al. 2014b; Xue et al. 2016; Shen et al. 2017; Chen et al. 2019a; Hou et al. 2021; Lu et al. 2022; Ding & Zhang 2024; Duan et al. 2024b). Moreover, bright plasma blobs can also be observed within the current sheet, as indicated by the pink arrows in Figure (d), as reported by previous studies (e.g., Li et al. 2016; Yan et al. 2022; Hou et al. 2024; Nóbrega-Siverio et al. 2025; Tang et al. 2025). The plasma blobs may be generated during the interchange reconnection as a result of tearing instability, as indicated by the simulation studies conducted by Bhattacharjee et al. (2009). As the interaction becomes more dynamic, a common footpoint region shared by the emerged loop and the newly formed loops is observed, collectively displaying a fan-spine-like morphology, as outlined by dashed lines in Figure 2 (e). The interaction between this newly emerging magnetic flux and the adjacent background field evolves into a fan-spine morphology, consistent with the

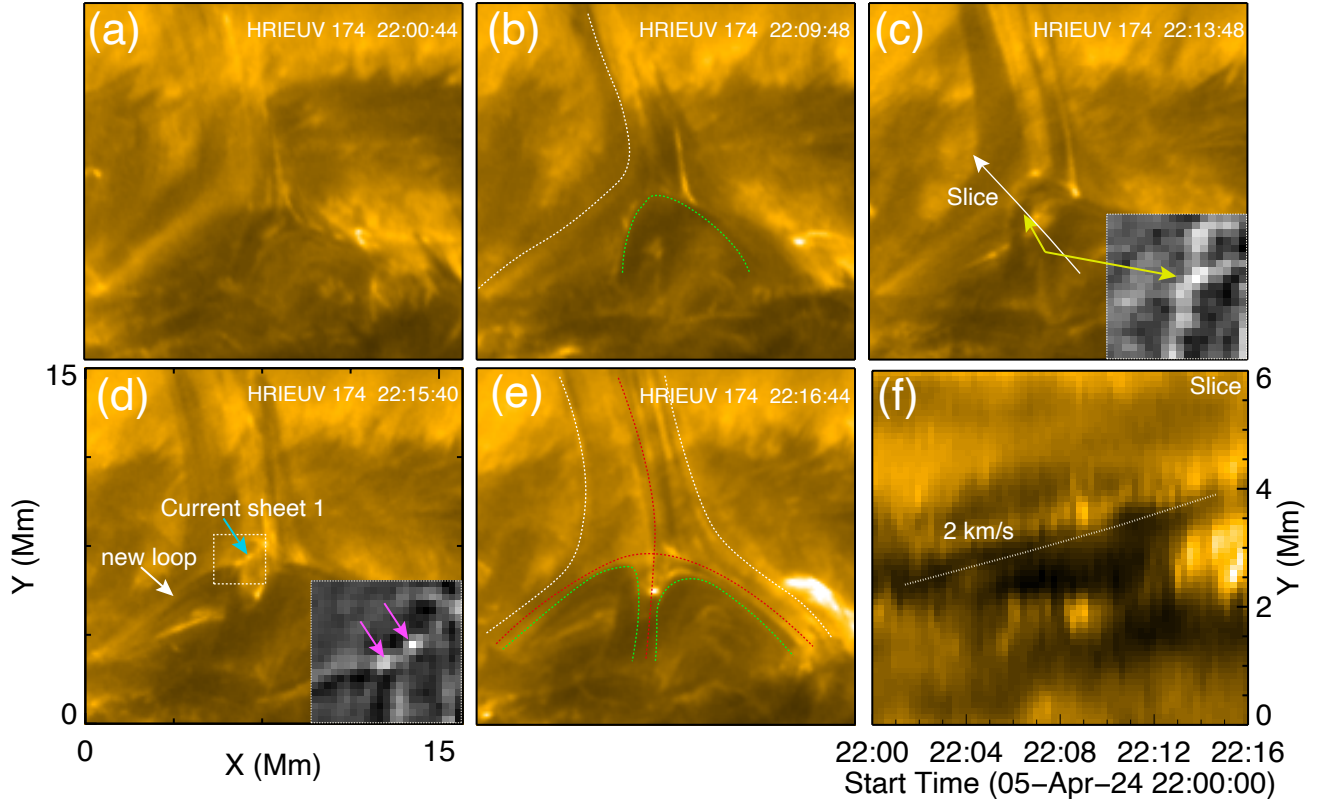


**Fig. 2.** (a)–(e):  $\text{HRI}_{\text{EUV}} 174\text{\AA}$  sequence images depicting the evolution process of the fan-spine-like topology. In panel (b), the emerged and ambient open field are outlined by green and white dashed lines, respectively. The yellow arrows point to the X point of reconnection between the emerging field and the surrounding open magnetic field in panel (c). The pink arrows denote the plasma blobs in a current sheet 1 (d). Panel (e): the fan surface and spine of the fan-spine-like structure are outlined by red dashed lines, while the green and white dashed lines outline the closed magnetic flux under the fan dome and open flux above the fan dome, respectively. Panel (f): the time-distance diagram along the direction of the white line in panel (c). An animation of the whole evolution process of the fan-spine system is available from 22:00 UT to 22:58 UT. The duration of the animation is 9 s.

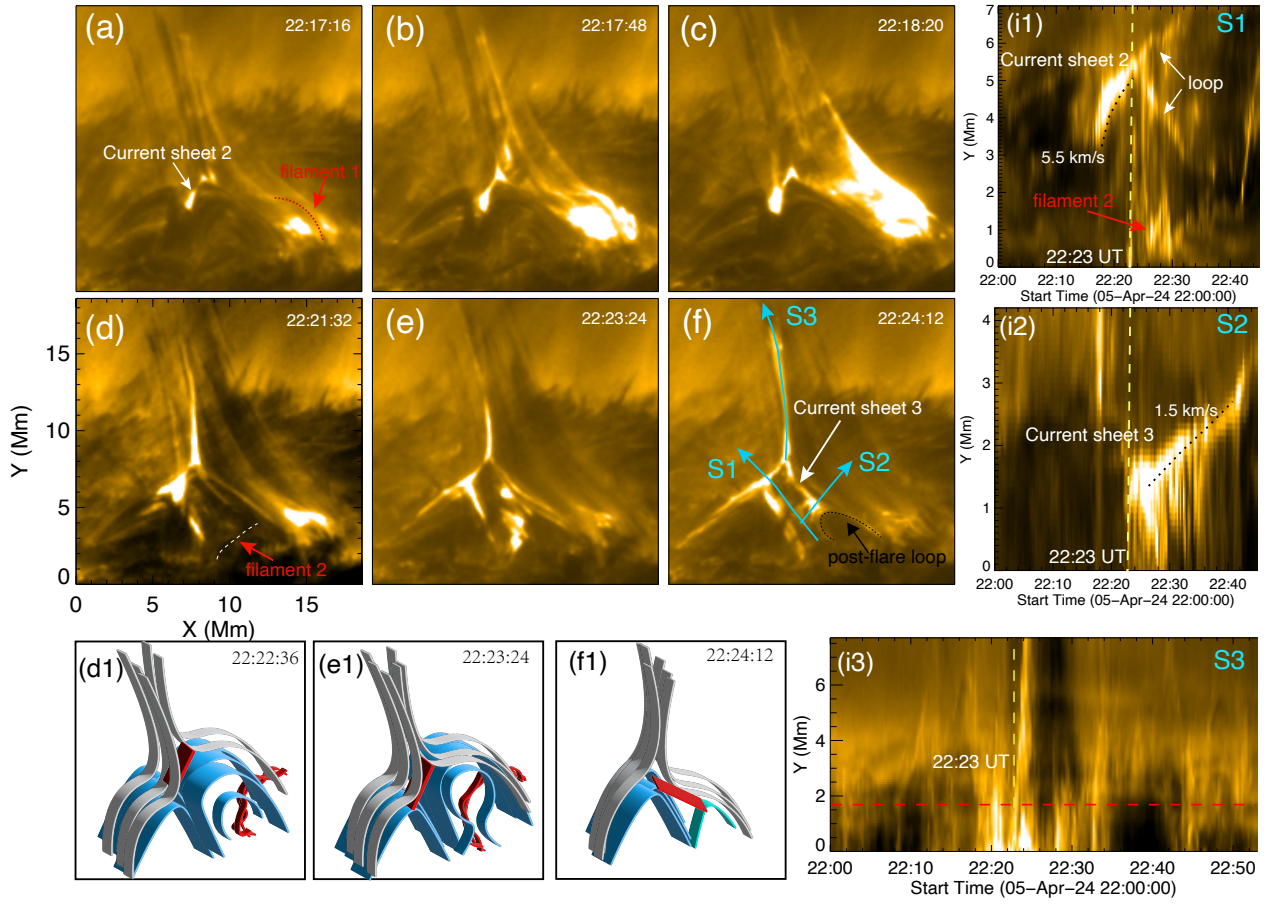
previous work of Török et al. (2009) and Duan et al. (2024b). In this event, due to the position of our interested event at the solar western limb, lacking the magnetic field data, we cannot employ magnetic field extrapolation. Thus, we refer to this event as the fan-spine-like structure.

Figure 3 presents the observational dynamic features associated with the transition from current sheet 2 (CS2) to current sheet 3 (CS3). At about 22:17:16, a bright emission appears beneath filament 1, located at the side of the fan-spine-like structure. Meanwhile, a CS2 feature appears within the fan-spine-like structure. Although the EUV image only provides the projected trajectory of filament 1 and CS2, it is clear that they move upward together (see the animation). The upward movement of the CS2 could be a reflection of larger-scale magnetic field relaxation in that region. Ultimately, filament 1 erupts, as evidenced by its structural changes from a closed magnetic flux system to an open field, as displayed in Figure 3 (c). Another filament (filament 2) is observed at 22:21:32 UT. About two minutes later, filament 2 is activated and erupts in the direction of CS2. This result may be triggered by CS2, effectively eliminating the restraining magnetic arcade overlaying the underlying filament 2. At 22:24:12 UT, a bright linear feature, indicated by the white arrow, forms a connection between the base of the jet spire and the top of the post-flare arcade. This feature is similar to the flare current sheet formed in the wake of the filament eruption (Antiochos et al. 1999; Wyper et al. 2017), referred to as the

CS3. Figure 3 (d1)–(f1) exhibits the schematic diagrams corresponding to panels (d)–(f) and the possible connectivity of filament 2.

By constructing a time–distance diagram along the arrow S3 (see Figure 3 (f)), it can be observed continuous occurrence of plasma outflows and a significant jet eruption ( $\sim 22:23$  UT), as displayed in Figure 3 (i3). We also employed the wavelet and Fourier analysis method (Torrence & Compo 1998; Auchère et al. 2016) to obtain the periods of the continuous plasma outflows. We extracted a light curve from S3, with the location marked by the red dashed line in Figure 3 (i3). The result is illustrated in Figures 7 (a1)–(a3). The speeds of these plasma outflows are presented in the time-distance diagram along the ejection to the highest position, as exhibited in Figures 6 (a) and (d).

Figure 3 (i1) and (i2) show the time–distance diagrams along cyan arrows S1 and S2 in panel (f). At around 22:23 UT, it can be clearly seen that CS2 transforms into a two-loop system moving in different directions (see the animation), while CS3 appears. It is worth noting that at this moment, filament 2 erupts toward CS2, as indicated by the red arrow in Figure 3 (i1). CS2 is observed from approximately 22:17 UT to 22:23 UT, during which its width ranged from 0.6 to 0.8 Mm, consistent with prior statistical analyses (Ding & Zhang 2024; Ding et al. 2024). The length of CS2 seems to grow over time, from an initial 3 Mm to a final 5 Mm before disappearing. According to the Sweet-Parker



**Fig. 3.** (a)–(f): HRI<sub>EUV</sub> 174Å sequence images showing the production of two current sheets. (d1)–(f1): schematic diagrams depicting the evolutionary sequence of filament 2, corresponding to the respective time instances shown in panels (d)–(f). (i1)–(i3) time-distance diagrams along the direction of the cyan arrows in panel (f). The black dashed line outlines the post-flare loop after the eruption of filament 2 in panel (f). The red dashed line in panel (i3) represents the position from which the light curve was extracted for wavelet analysis, with the results presented in Figures 7 (a1)–(a3).

mechanism (Priest & Forbes 2000), the reconnection rate (the inflow Alfvén Mach number ( $M_A$ )) is theoretically proportional to the ratio of the current sheet thickness ( $d$ ) to its length ( $L$ ) (e.g., Xue et al. 2016; Chen et al. 2019a; Yang et al. 2024b). Based on these measurements, the reconnection rate of the CS2 is estimated to be in the range of 0.12 to 0.2. During the period from 22:23 to 22:40 UT, CS3 displayed a width of approximately 0.4 Mm to 0.6 Mm, while its length varied from 2.7 Mm to 7.4 Mm. Unlike CS2, CS3 exhibited a contraction phase following its initial elongation. The estimated reconnection rate of CS3 ranged from 0.12 to 0.17. Both current sheets show an upward movement trend, with CS2 and CS3 moving at speeds of 5.5 km/s and 1.5 km/s, respectively.

Figure 4 illustrates the dynamic evolution of the interchange reconnection in the outflow region of CS3. A set of magnetic loops is clearly visible to the left of the jet spine, as shown in Figure 4(a). These loops are reconnected loops formed in the outflow region of CS2. At 22:25:16 UT, this set of magnetic loops clearly exhibits three distinct groups of field lines, indicated by the yellow arrows. Between 22:24:28 UT and 22:25:32 UT, these loops move toward the jet’s spine, exhibiting a slipping motion. They reconnect with the surrounding open field lines at CS3, with the reconnection point indicated by the purple arrow in panel (d). At 22:26:36, the newly formed loops after

interchange reconnection are shown by the cyan arrow. Eventually, the closed field lines on the left of the jet spine change into open field lines through the dynamic evolution of interchange reconnection, revealing a curtain-like feature (see panels (f)–(i)). The width of this curtain-like feature is approximately 1.7 Mm. By constructing a time-distance diagram along the curtain-like structure from arrows S4–S6, we can observe the continuous plasma outflows along the curtain feature. The average velocity of these plasma outflows is  $\sim 80 \text{ km s}^{-1}$ . We extracted the light curves from S4, S5, and S6, with the location marked by the red dashed lines in Figures 4 (i1)–(i3). The results of wavelet and Fourier analysis are shown in Figures 7 (b)–(d).

Figure 5 shows the ultimate breakdown process of this fan-spine-like system. CS3 gradually approaches the post-flare loop, as shown in Figure 5 (a)–(c). This may result from the migration of the null point in the fan-spine system, caused by changes in gas pressure and magnetic pressure. Subsequently, another filament, referred to as filament 3, appears below the post-flare loop, as displayed in Figure 5 (d). Together, they exhibit dynamic evolutionary characteristics of uplift and interact with each other (see Figure 5 (e)). Eventually, the post-flare loop and filament 3 transition from closed magnetic flux to open flux at 22:47:40 UT.

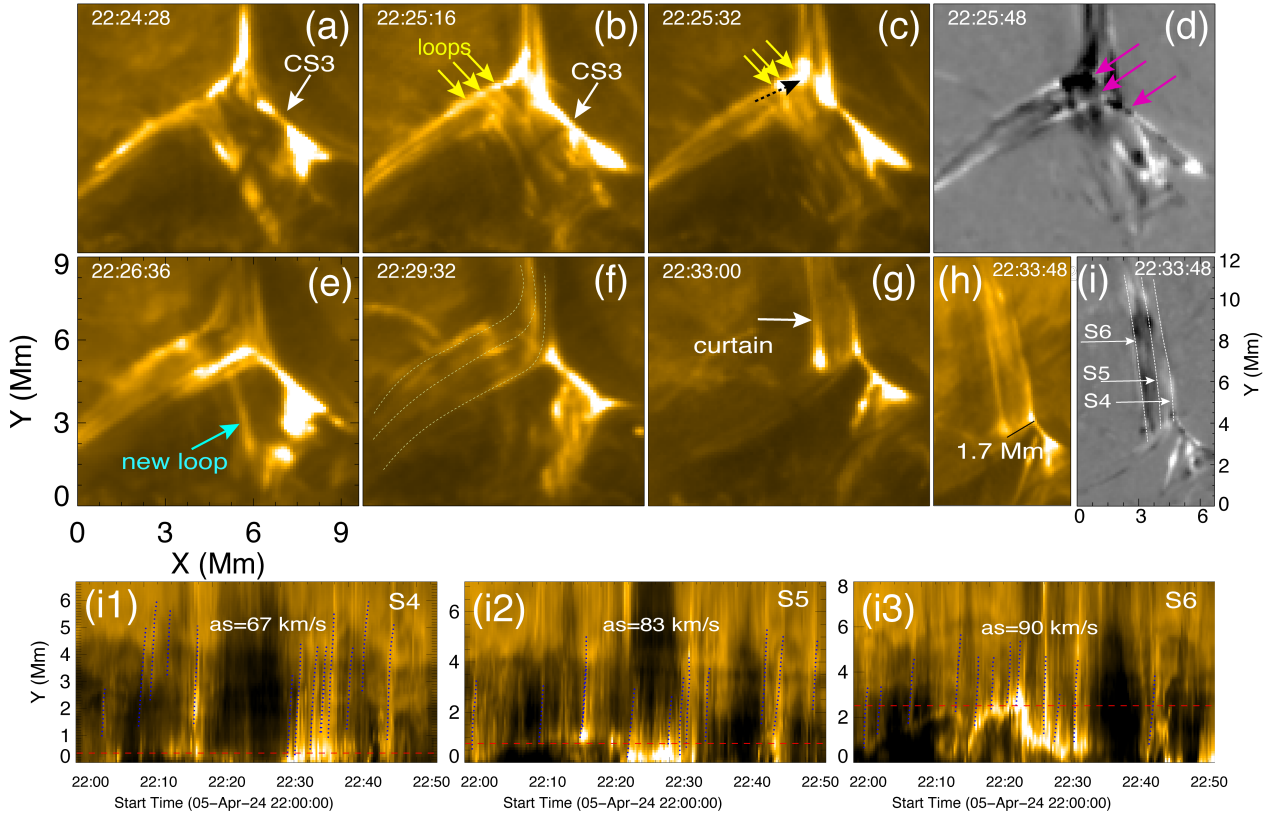


**Fig. 4.** (a)–(f): A sequence of  $\text{HRI}_{EUV}$  174 Å images illustrating the continuous interchange reconnection process. (b) The yellow arrows indicate three groups of loops. (c) The black dashed arrow shows the slipping motion of these three loops. (d) The pink arrows denote the reconnection site between these three loops and the ambient open fields. The yellow dashed lines outline the open magnetic field lines of the three loops after the reconnection in panel (f). Panels (g)–(i) show a curtain-like feature. (i1)–(i3): Time-distance diagrams along the direction of the white dashed lines in panel (i). The dotted blue lines in panels (i1)–(i3) trace the inclined ridges that correspond to the plasma outflows along the curtain feature. The speeds were calculated by performing a linear fit on the height-time measurements. The “as” is an abbreviation for “average speed”. The red dashed lines in panels (i1)–(i3) mark the locations from which the light curves were extracted for wavelet analysis, with the results presented in Figure 7 (b) to (d).

Figure 6 illustrates the spatial relationship between the fan-spine-like structure and the surrounding magnetic field. To enhance the visibility of this structure,  $\text{HRI}_{EUV}$  174 Å images are superimposed on a sequence of FSI 174 Å images, see Figure 6 (b1)–(b3). Additionally, running difference images from the FSI 304 Å sequence, shown at 10-minute intervals, depict the process of plasma outflow. To quantify the plasma motion, two cuts were placed, as shown in Figure 6 (a). It should be noted that Slice 1 is positioned along the path where the plasma ejection reaches its maximum height within the fan-spine-like structure, while Slice 2 is established in the direction of the eruption of filament 1 along the side of this structure. By calculating the light curve within the yellow dashed box in Figure 6 (a), we found that the peak of this intensity curve corresponds to the eruption of filament 1. Based on the time-distance diagram of Figure 6 (e), we determined that the time and speed of the erupted filament 1 are about 22:18 UT and  $186 \text{ km s}^{-1}$ , respectively. The average speed of the recurring plasma ejections is  $64 \text{ km s}^{-1}$ . The highest plasma ejection occurred around 22:23 UT (see Figure 6 (d)), corresponding to the eruption of filament 2 in Figures 3 (d)–(f) and (i3). In the FSI 304 Å running difference images, it can be observed that the plasma material flows along the closed field lines and finally impacts the solar surface, as denoted by white arrows in Figure 6 (c2) and (c3). No disturbance signals were

observed in the  $\text{HRI}_{EUV}$  174 Å or FSI 174 Å images, indicating that the temperature of the material flows is not high relative to the coronal loop. Due to the low temporal resolution of the FSI, it is not possible to distinguish which filament eruption the material propagating along the closed magnetic field lines in Figure (c2)–(c3) originates from. However, these results indicate that the reconnection occurring in the low corona can contribute to supplying material and energy to the high corona. Additionally, the ejected plasma flows subsequently fall down, possibly corresponding to coronal rain within the coronal loops. The ongoing coronal rain can indicate the spatial distribution of heating of the coronal loops (Antolin et al. 2010; Antolin & Froment 2022).

In Figure 7, to investigate the periodic oscillation of plasma outflows along the jet spire and the curtain feature, we applied wavelet and Fourier analysis to four light curves, following the methodology introduced by Torrence & Compo (1998) and Auchère et al. (2016). The positions from which the light curves were extracted are marked by the red dashed lines in Figure 3 (i3) and Figures 4 (i1)–(i3). We chose to fit the fast Fourier transform (FFT) of each light curve using the following power-law equation:

$$\sigma(\nu) = A\nu^s + BK_p(\nu) + C \quad (1)$$

where  $\nu$  is the Fourier frequency; A, B, and C are constants; the second term accounts for the possible presence of pulses in the

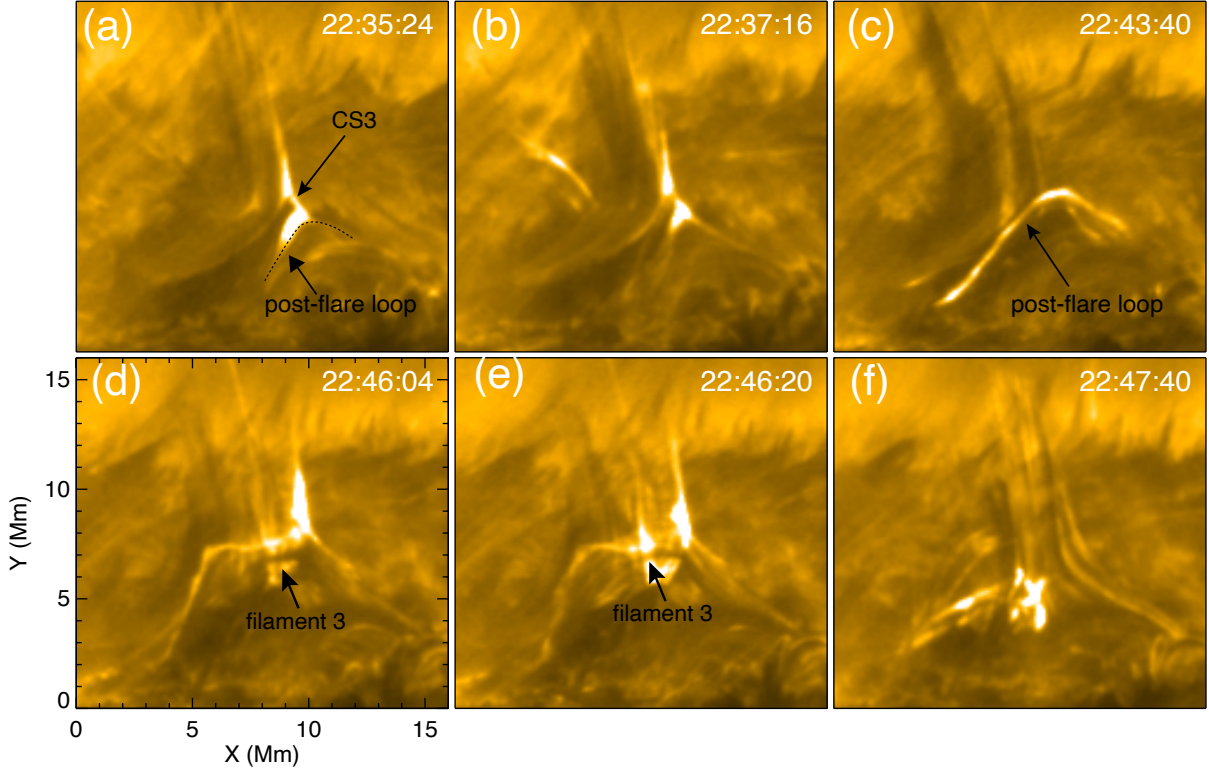


**Fig. 5.** Panels (a)–(f) illustrate the final evolution process of the fan-spine-like system. The black arrows denote another filament (filament 3) in panels (d)–(e).

time series;  $K_\rho(\nu)$  is the Kappa function:

$$K_\rho(\nu) = \left(1 + \frac{\nu^2}{\kappa\rho^2}\right)^{-\frac{\kappa+1}{2}} \quad (2)$$

where  $\rho$  is the width of the power spectral distribution (PSD) and  $\kappa$  defines the extent of its high-frequency wing.

As shown in Figures 7 (a3)–(d3), the global 99% Fourier confidence level exhibits higher values compared to the local and global 99% wavelet confidence levels. The global 99% wavelet confidence levels are higher than the local 99% wavelet confidence level. This result is consistent with findings reported in previous studies (e.g., Auchère et al. 2016; Kayshap et al. 2020; Li 2022; Mandal et al. 2022). In Figure 7 (a3), (c3), and (d3), a slope variation of the Fourier spectrum forms a peak around  $5 \times 10^3 \mu\text{Hz}$ , corresponding to a period of 200 s. This indicates that periodic interchange reconnection occurs on the curtain structure (Figure 7 (b3), (c3), and (d3)), comparable to the periodicity of interchange reconnection at the spire of the jet (Figure 7 (a3)), with both being approximately 200 s. It should be noted that during the eruption, the upward movement of cold plasma obscures the hot plasma outflows. This may explain the lack of a distinct periodicity in Figure 7 (b3). In this scenario, the periodicity of the interchange reconnection may also be underestimated.

#### 4. Conclusion and Discussion

Using high spatial resolution observations from the Extreme Ultraviolet Imager (EUI) onboard the Solar Orbiter, we report direct imaging of three current sheets (CSs), associated with recurrent interchange reconnection near the null point within a fan-spine-like system. Three current sheets occurring near the null

point are modulated by emerged small magnetic structures. CS1 is generated by the interaction between emerging magnetic loops and the ambient magnetic field. The X point at the reconnection site and plasma blobs within CS1 are observed. CS2 appears to be influenced by the eruption of filament 1 on the side of the fan-spine-like topology, lasting about 6 minutes with a maximum length of 5 Mm and a width of 0.8 Mm. The formation mechanism of CS3 is similar to the flare current sheet in the breakout jet model. CS3 lasts 17 minutes with a maximum length of 7.4 Mm and a width of 0.6 Mm. The estimated reconnection rates are approximately 0.12 to 0.2 for the CS2 and 0.12 to 0.17 for the CS3. A curtain-like feature with a width of 1.7 Mm is presented during the dynamic evolution of the fan-spine system. Periodic interchange reconnection occurs in the curtain, with a periodicity comparable to that of interchange reconnection at the jet spire, both being about 200 s. Additionally, the plasma outflows from periodic reconnections, regardless of where they occur, nearly encompass the evolution of the fan-spine system, exhibiting a gradual physical process similar to that of interchange reconnection in a pseudo-streamer. We suggest that the dynamics of re-current magnetic reconnection in such a small fan-spine system might be more complex than we recognized before. Our results reveal a self-similarity between small-scale fan-spine structures and large-scale pseudo-streamer structures.

In our research, we found that during the dynamic evolution of the fan-spine system, complex magnetic field interchange reconnection occurs near the null point. Specifically, the appearance of CS1 results from the interchange reconnection between the newly emerging magnetic flux and background fields (Figure 2); the transition from CS2 to CS3 is accompanied by exchanges in reconnection outflows and inflows (Figure 3); interchange reconnection occurs between the closed magnetic loop

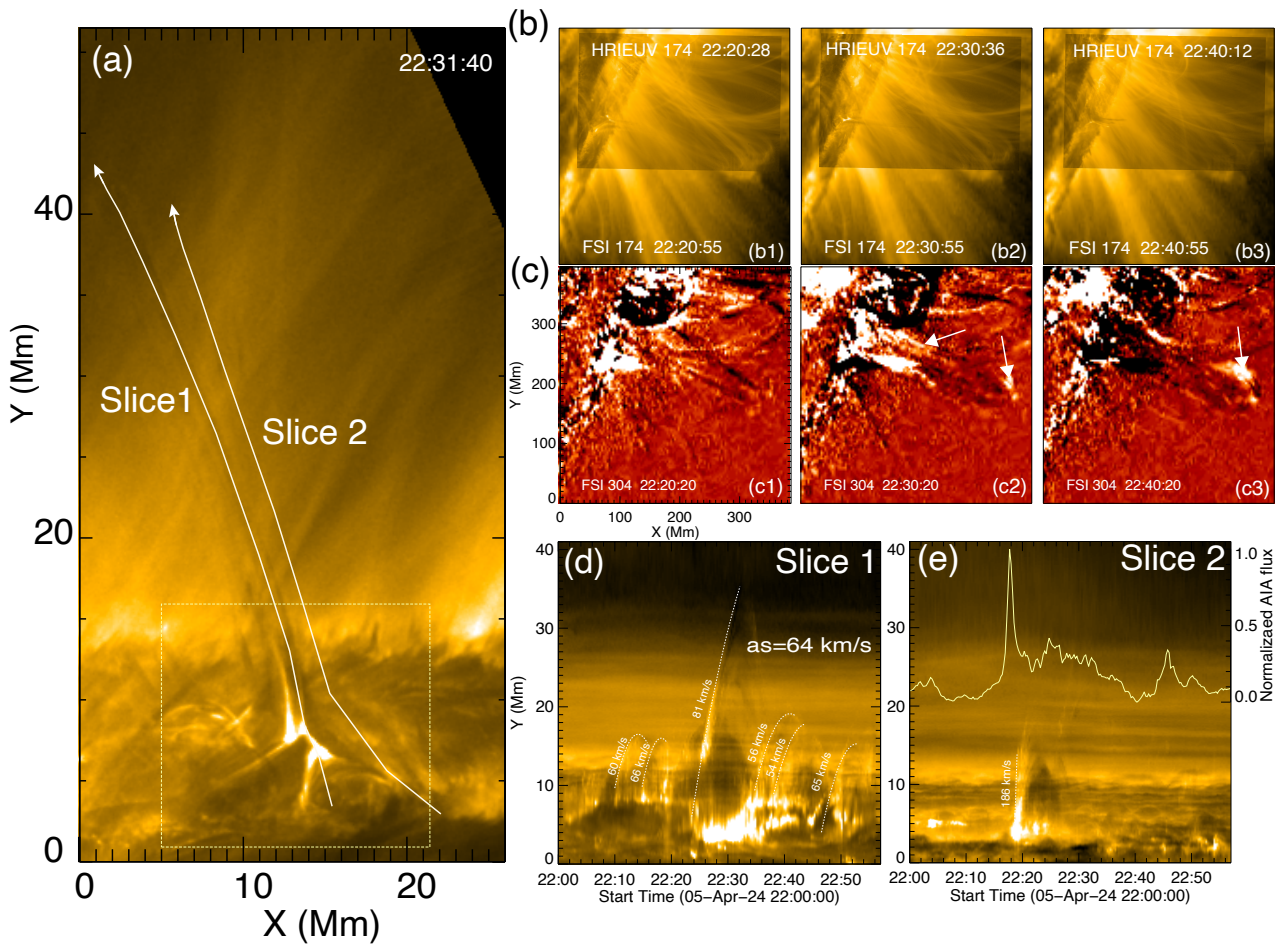


**Fig. 6.** In panel (a), the white arrow (Slice 1) indicates the direction in which plasma outflow is ejected to its highest position. Slice 2 is along the direction of the eruption of filament 1 on the side of the fan-spine structure. (b)–(c) The HRI<sub>EUV</sub> images are overlaid on the FSI<sub>174</sub> images and FSI<sub>304</sub> running difference images, showing the location of the fan-spine-like structure. The white arrows illustrate the plasma ejection material propagating along the closed magnetic field lines in panel (c2)–(c3). In panels (d)–(e), the time–distance intensity diagrams of HRI<sub>EUV</sub> 174 Å are plotted along Slice 1 and Slice 2 in panel (a). The yellow curve represents the EUV 174 Å light curve, which is calculated within the yellow dashed box in panel (a) from 22:00 UT to 22:57 UT.

under the fan dome and the surrounding open field, forming a curtain-like structure in the reconnection outflow region of CS3 (Figure 4); and periodic reconnection occur near the null point, including on the jet spine and the curtain feature. These results suggest that the magnetic reconnection in a fan-spine topology seems to be more complex than single null-point reconnection, possibly involving QSL reconnection or separators (i.e., a series of nulls). As shown in Duan et al. (2024b), they found that two null points can be connected by an elongated sheetlike quasi-separatrix layer (QSL) through the magnetic null point tracing method and the calculation of the 3D squashing factor  $Q$ . This result indicates the possible existence of multiple magnetic null points in the fan-spine system.

High-resolution EUV 174 Å images reveal that persistent plasma outflows occur near the magnetic null point. The velocity of these plasma outflows ( $\sim 64\text{--}90\text{ km s}^{-1}$ ) is relatively lower compared to the filament 1 eruption (i.e.,  $186\text{ km s}^{-1}$ ), indicating that gentle reconnection occurs persistently near the magnetic null point. The recurrent reconnection that persistently occurs near the magnetic null point in the fan-spine configuration, resulting in plasma outflows, has also been reported by previous studies (Cheng et al. 2023; Duan et al. 2024b; Kumar et al.

2024). This process may resemble the simulations by Nóbrega-Siverio & Moreno-Insertis (2022); Nóbrega-Siverio et al. (2023), where stochastic granular motions are sufficient to stress the small-scale fan-spine structure, triggering sustained reconnection at the coronal null point, which naturally results in persistent jetting activity manifested in the form of recurrent, gentle plasma outflows. The gentle reconnection or gentle plasma outflows most likely result from the interchange reconnection between magnetic flux under the fan dome and the ambient open magnetic field lines. Such gradual physical processes are similar to the interchange reconnection occurring in the pseudo-streamer structure (e.g., Masson et al. 2014) and may play a critical role in the continuous energy and material injection into the high corona.

The observation that sparked our interest in this event was the identification of two distinct current sheets (CS2 and CS3) at disparate locations. It is pertinent to note that changes in magnetic pressure or gas pressure may lead to reconnection reversals (Murray et al. 2009), resulting in the formation of oscillatory current sheets around the null point, as demonstrated by Hong et al. (2019). Their study focused on oscillatory magnetic reconnection preceding a jet within the breakout current sheet. Here,

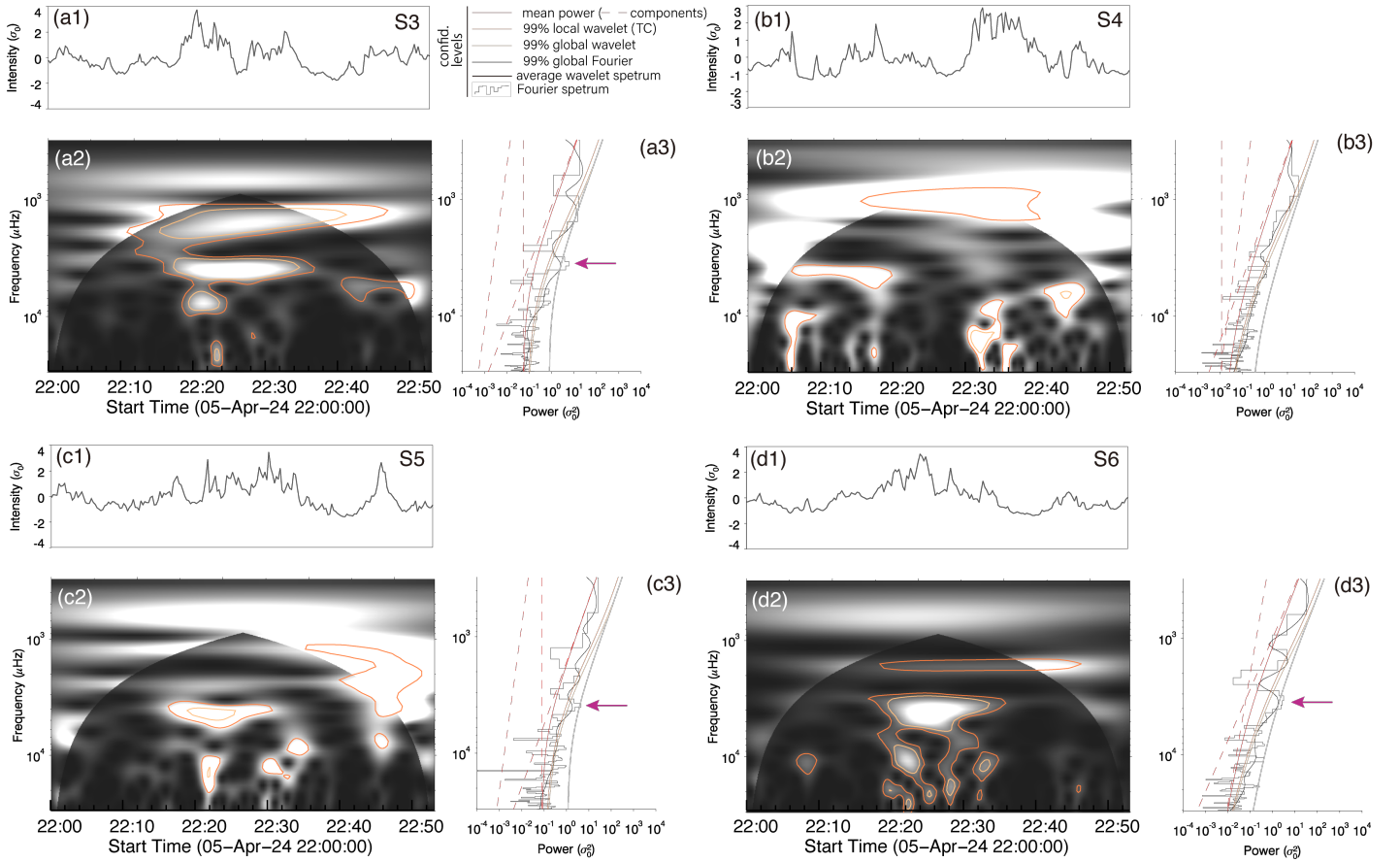


**Fig. 7.** Wavelet and Fourier analysis of the temporal evolution for plasma outflows (Figure 3 (i3)) and curtain feature (Figures 4 (i1)–(i3)). In the upper left corner of each panel, the variance-normalized light curve is displayed. Panels (a2), (b2), (c2), and (d2) illustrate the whitened Morlet wavelet spectrum, which is normalized according to the background power model. The Fourier power spectra (black histogram), time-averaged wavelet spectrum (thick line), and fitted noise model (red line), along with its components (dashed red line), are shown in panels (a3), (b3), (c3), and (d3). 99% local and global confidence levels with fitted noise are shown in dark and light orange curves, respectively. The grey line indicates the 99% global confidence level for the Fourier spectrum. The peak of the Fourier power is labeled with pink arrows.

the appearance of CS2 and CS3 in sequence also indicates the reconnection reversal. However, it should be attributed to the dynamics described by the breakout jet model, different from the oscillatory reconnection. In simulations conducted by Wyper et al. (2017), shear facilitated the accumulation of free energy within the filament channels along the polarity inversion line of the fan-spine magnetic configuration. As shear progressed, the overlying magnetic field expanded upward, leading to the formation of a breakout current sheet (BCS) at the null point. In this event, the appearance of CS2 is influenced by the eruption of filament 1 on the side of the fan-spine-like structure. Reconnection at the CS2 then eliminates the restraining fields, resulting in the eruptions of another filament (filament 2) (e.g., Wyper et al. 2017, 2018; Kumar et al. 2018; Sun et al. 2023; Duan et al. 2024a,b; Yang et al. 2024b). Filament 2 then rapidly reconnected with the external open field, inducing explosive interchange reconnection within the CS3 left in its wake, thereby producing the post-flare loops. The transition from CS2 to CS3 in this event is similar to the breakout jet model (Wyper et al. 2017). In the simulation studies (e.g., Scott et al. 2021), the reversal or transition of such current sheets seems not to have been considered. Our observations may also indicate that the dynamics of large-scale pseudo-streamer structures could undergo similar complex processes, which might be a possible reason for the appearance of complex structures in the solar wind.

It should be noted that our calculations of the width of the current sheet may overestimate the actual width because the features we observed are essentially plasma sheets embedded within the current sheet (e.g., Lin et al. 2015). What we are calculating here is the upper limit of the width of the current sheet. Considering that the thermal halo effect has minimal impact, the lengths of the current sheets are generally comparable to the lengths of the plasma sheets. Therefore, the calculated value of reconnection rate is likely overestimated, representing only an upper limit of the true reconnection rate. However, the overall trend reflects the evolutionary characteristics of the reconnection rate.

In the large-scale pseudo-streamer structures, the separatrix curtain formed by the separatrix fan surface from the central null is orthogonal to the other two surfaces and is bounded by their respective spine field lines (Titov et al. 2011). Compared to the fan-spine topology (often described as a separatrix dome with a single null point), separatrix curtains involve multiple null points connected by separators. In fact, considering the three-dimensional invariance of the fan-spine structure in a two-dimensional geometry, the three-dimensional null point is replaced with a separator, and the spine line is replaced with a spine surface. Within the three-dimensional magnetic reconnection framework, reconnection is not confined to null points but occurs throughout a finite diffusion region (Pontin

& Priest 2022). In this scenario, the fan-spine structure resembles a scaled-down version of the pseudostreamer structure (e.g., Lynch & Edmondson 2013; Wyper et al. 2024). In the small-scale fan-spine topology, the presence of multiple nulls and connecting separators allows for more frequent and complex interchange reconnection between open and closed magnetic fluxes, similar to the pseudo-streamer simulated by Scott et al. (2021). Consistent with our previous findings (Duan et al. 2024b), our current observations reveal the occurrence of complex and frequent interchange reconnection in the coronal jets between open and closed magnetic fluxes, likely mediated by multiple null points. Concurrently, the coronal jet expelled plasma with a curtain-like jet spire and complex current sheet evolution. These results provide evidence that this coronal jet occurs in a small-scale separatrix curtain, resembling a scaled-down version of the pseudostreamer structure. Similarly, Mandal et al. (2022) recently reported analogous phenomena, including a curtain-like jet spire and numerous complex morphological changes, in a highly dynamic, small-scale event observed by EU1 in a polar coronal hole. Moreover, Li et al. (2025a) also reconstructed a separatrix curtain-like magnetic topology in small-scale recurrent jets. These high-resolution EU1 imaging observations jointly reinforce the view of the across-scale self-similarity of magnetic separatrix curtains and their associated interchange reconnection processes from the large-scale pseudo-streamers down to the tiny coronal jets.

**Acknowledgements.** The authors are grateful for the helpful discussions with Prof. Hui Tian from Peking University and Yuandeng Shen from Harbin Institute of Technology, and the anonymous referee's valuable comments and suggestions. This work is supported by the Strategic Priority Research Program of the Chinese Academy of Sciences, Grant No. XDB0560000, NSFC grant 12403065 & 12425301, Beijing Natural Science Foundation (1244053). X.L.Y. was supported by the National Science Foundation of China (NSFC) under Nos. 12325303, Yunnan Key Laboratory of Solar Physics and Space Science under No. 202205AG070009, and Yunnan Fundamental Research Projects under Nos. 202301AT070347 and 202301AT070349. H.C.C. was supported by NSFC grant (12573061) and the Yunnan Fundamental Research Projects under Nos. 202401CF070165. J.C.H. was supported by the NSFC grant 12173084, the CAS "Light of West China" Program, and the Yunnan Science Foundation of China (202401AT070071). Z.Y.H. was supported by NSFC grant 12303057. J.C.W. was supported by the Yunnan Fundamental Research Projects under Nos. 202501AW070002. The authors are grateful for the data provided by the Solar Orbiter science teams. Solar Orbiter is a mission of international cooperation between ESA and NASA, operated by ESA. The EU1 instrument was built by CSL, IAS, MPS, MSSL/UCL, PMOD/WRC, ROB, LCF/IO with funding from the Belgian Federal Science Policy Office (BELSPO/PRODEX PEA 4000112292); the Centre National d'Etudes Spatiales (CNES); the UK Space Agency (UKSA); the Bundesministerium für Wirtschaft und Energie (BMWi) through the Deutsches Zentrum für Luftund Raumfahrt (DLR); and the Swiss Space Office (SSO).

## References

Antiochos, S. K., DeVore, C. R., & Klimchuk, J. A. 1999, *ApJ*, 510, 485  
 Antiochos, S. K., Mikić, Z., Titov, V. S., Lionello, R., & Linker, J. A. 2011, *ApJ*, 731, 112  
 Antolin, P. & Froment, C. 2022, *Frontiers in Astronomy and Space Sciences*, 9, 820116  
 Antolin, P., Shibata, K., & Vissers, G. 2010, *ApJ*, 716, 154  
 Auchère, F., Froment, C., Bocchialini, K., Buchlin, E., & Solomon, J. 2016, *ApJ*, 825, 110  
 Bale, S. D., Badman, S. T., Bonnell, J. W., et al. 2019, *Nature*, 576, 237  
 Bhatnagar, A., Prasad, A., Nóbrega-Siverio, D., Rouppe van der Voort, L., & Joshi, J. 2025a, *A&A*, 698, A174  
 Bhatnagar, A., Prasad, A., Rouppe van der Voort, L., Nóbrega-Siverio, D., & Joshi, J. 2025b, *A&A*, 693, A221  
 Bhattacharjee, A., Huang, Y.-M., Yang, H., & Rogers, B. 2009, *Physics of Plasmas*, 16, 112102  
 Bruzek, A. 1967, *Sol. Phys.*, 2, 451  
 Chen, H., Yang, J., Duan, Y., & Ji, K. 2019a, *ApJ*, 879, 74

Chen, H., Yang, J., Yang, B., Ji, K., & Bi, Y. 2018, *Sol. Phys.*, 293, 93  
 Chen, Y., Tian, H., Zhu, X., et al. 2019b, *Science in China E: Technological Sciences*, 62, 1555  
 Cheng, X., Priest, E. R., Li, H. T., et al. 2023, *Nature Communications*, 14, 2107  
 Chitta, L. P., Peter, H., Young, P. R., & Huang, Y. M. 2017, *A&A*, 605, A49  
 Chitta, L. P., Seaton, D. B., Downs, C., DeForest, C. E., & Higginson, A. K. 2023, *Nature Astronomy*, 7, 133  
 Crooker, N. U., Gosling, J. T., & Kahler, S. W. 2002, *Journal of Geophysical Research (Space Physics)*, 107, 1028  
 Ding, T. & Zhang, J. 2024, *ApJ*, 974, 104  
 Ding, T., Zhang, J., Fang, Y., & Ma, Z. 2024, *ApJ*, 964, 58  
 Duan, Y., Shen, Y., Chen, H., et al. 2023, *ApJ*, 942, L22  
 Duan, Y., Shen, Y., Tang, Z., Zhou, C., & Tan, S. 2024a, *ApJ*, 968, 110  
 Duan, Y., Shen, Y., Zhou, X., et al. 2022, *ApJ*, 926, L39  
 Duan, Y., Tian, H., Chen, H., et al. 2024b, *ApJ*, 962, L38  
 Færder, Ø. H., Nóbrega-Siverio, D., Carlsson, M., & Martínez-Sykora, J. 2024, *A&A*, 687, A171  
 Fisk, L. A., Schwadron, N. A., & Zurbuchen, T. H. 1998, *Space Sci. Rev.*, 86, 51  
 Fuentes-Fernández, J. & Parnell, C. E. 2013, *A&A*, 554, A145  
 Hong, J., Jiang, Y., Yang, J., Li, H., & Xu, Z. 2017, *ApJ*, 835, 35  
 Hong, J., Yang, J., Chen, H., et al. 2019, *ApJ*, 874, 146  
 Hou, Y., Li, T., Yang, S., & Zhang, J. 2019, *ApJ*, 871, 4  
 Hou, Z., Tian, H., Chen, H., et al. 2021, *ApJ*, 915, 39  
 Hou, Z., Tian, H., Madjarska, M. S., et al. 2024, *A&A*, 687, A190  
 Jiang, C., Feng, X., Wu, S. T., & Hu, Q. 2013, *ApJ*, 771, L30  
 Kayshap, P., Srivastava, A. K., Tiwari, S. K., Jelínek, P., & Mathioudakis, M. 2020, *A&A*, 634, A63  
 Krucker, S., Kontar, E. P., Christe, S., Glesener, L., & Lin, R. P. 2011, *ApJ*, 742, 82  
 Kumar, P., Karpen, J. T., Antiochos, S. K., et al. 2018, *ApJ*, 854, 155  
 Kumar, P., Karpen, J. T., Uritsky, V. M., et al. 2022, *ApJ*, 933, 21  
 Kumar, P., Karpen, J. T., Yurchyshyn, V., DeVore, C. R., & Antiochos, S. K. 2024, *ApJ*, 973, 74  
 Li, D. 2022, *A&A*, 662, A7  
 Li, L., Zhang, J., Peter, H., et al. 2016, *Nature Physics*, 12, 847  
 Li, T., Priest, E., & Guo, R. 2021, *Proceedings of the Royal Society of London Series A*, 477, 20200949  
 Li, T., Yang, S., Zhang, Q., Hou, Y., & Zhang, J. 2018, *ApJ*, 859, 122  
 Li, X., Solanki, S. K., Wiegmann, T., et al. 2025a, *A&A*, 702, A201  
 Li, Z. F., Guo, J. H., Cheng, X., et al. 2025b, *A&A*, 696, L2  
 Lin, J., Murphy, N. A., Shen, C., et al. 2015, *Space Sci. Rev.*, 194, 237  
 Linker, J. A., Lionello, R., Mikić, Z., Titov, V. S., & Antiochos, S. K. 2011, *ApJ*, 731, 110  
 Liu, C., Deng, N., Liu, R., et al. 2015, *ApJ*, 812, L19  
 Liu, W., Berger, T. E., Title, A. M., Tarbell, T. D., & Low, B. C. 2011, *ApJ*, 728, 103  
 Long, D. M., Chitta, L. P., Baker, D., et al. 2023, *ApJ*, 944, 19  
 Lu, L., Feng, L., Warmuth, A., et al. 2022, *ApJ*, 924, L7  
 Lynch, B. J. & Edmondson, J. K. 2013, *ApJ*, 764, 87  
 Mandal, S., Chitta, L. P., Peter, H., et al. 2022, *A&A*, 664, A28  
 Masson, S., Aulanier, G., Pariat, E., & Klein, K. L. 2012, *Sol. Phys.*, 276, 199  
 Masson, S., McCauley, P., Golub, L., Reeves, K. K., & DeLuca, E. E. 2014, *ApJ*, 787, 145  
 Masson, S., Pariat, E., Aulanier, G., & Schrijver, C. J. 2009, *ApJ*, 700, 559  
 Müller, D., St. Cyr, O. C., Zouganelis, I., et al. 2020, *A&A*, 642, A1  
 Murray, M. J., van Driel-Gesztelyi, L., & Baker, D. 2009, *A&A*, 494, 329  
 Ning, Z., Wang, Y., Hong, Z., & Li, D. 2022, *Sol. Phys.*, 297, 2  
 Nóbrega-Siverio, D., Joshi, R., Sola-Viladesau, E., Berghmans, D., & Lim, D. 2025, *A&A*, 702, A188  
 Nóbrega-Siverio, D. & Moreno-Insertis, F. 2022, *ApJ*, 935, L21  
 Nóbrega-Siverio, D., Moreno-Insertis, F., Galsgaard, K., et al. 2023, *ApJ*, 958, L38  
 Pariat, E., Antiochos, S. K., & DeVore, C. R. 2009, *ApJ*, 691, 61  
 Pellegri-Franchon, T., Masson, S., Pariat, E., Wyper, P. F., & DeVore, C. R. 2023, *A&A*, 675, A55  
 Petrova, E., Van Doorselaere, T., Berghmans, D., et al. 2024, *A&A*, 687, A13  
 Pontin, D. I. & Priest, E. R. 2022, *Living Reviews in Solar Physics*, 19, 1  
 Pontin, D. I., Priest, E. R., & Galsgaard, K. 2013, *ApJ*, 774, 154  
 Priest, E. & Forbes, T. 2000, *Magnetic Reconnection: MHD Theory and Applications*  
 Priest, E. R. & Forbes, T. G. 2002, *A&A Rev.*, 10, 313  
 Rochus, P., Auchère, F., Berghmans, D., et al. 2020, *A&A*, 642, A8  
 Scott, R. B., Pontin, D. I., Antiochos, S. K., DeVore, C. R., & Wyper, P. F. 2021, *ApJ*, 913, 64  
 Seaton, D. B., De Groof, A., Shearer, P., Berghmans, D., & Nicula, B. 2013, *ApJ*, 777, 72  
 Shen, Y. 2021, *Proceedings of the Royal Society of London Series A*, 477, 217  
 Shen, Y., Liu, Y. D., Su, J., Qu, Z., & Tian, Z. 2017, *ApJ*, 851, 67  
 Shen, Y., Qu, Z., Zhou, C., et al. 2019, *ApJ*, 885, L11  
 Shibata, K., Ishido, Y., Acton, L. W., et al. 1992, *PASJ*, 44, L173

- Solanki, S. K., del Toro Iniesta, J. C., Woch, J., et al. 2020, *A&A*, 642, A11
- Song, Y. & Tian, H. 2018, *ApJ*, 867, 159
- Song, Y. L., Guo, Y., Tian, H., et al. 2018, *ApJ*, 854, 64
- Sterling, A. C. & Moore, R. L. 2020, *ApJ*, 896, L18
- Sterling, A. C., Moore, R. L., Panesar, N. K., & Samanta, T. 2020, in *Journal of Physics Conference Series*, Vol. 1620, *Journal of Physics Conference Series*, 012020
- Su, Y., Liu, R., Li, S., et al. 2018, *ApJ*, 855, 77
- Sun, X., Hoeksema, J. T., Liu, Y., et al. 2013, *ApJ*, 778, 139
- Sun, Z., Li, T., Tian, H., et al. 2023, *ApJ*, 953, 148
- Tan, S., Warmuth, A., Schuller, F., et al. 2025, *arXiv e-prints*, arXiv:2509.04771
- Tang, Z., Shen, Y., Liu, D., et al. 2025, *ApJ*, 990, L16
- Tian, H., DeLuca, E. E., Cranmer, S. R., et al. 2014a, *Science*, 346, 1255711
- Tian, H., Li, G., Reeves, K. K., et al. 2014b, *ApJ*, 797, L14
- Tian, H., Yurchyshyn, V., Peter, H., et al. 2018, *ApJ*, 854, 92
- Titov, V. S., Mikić, Z., Linker, J. A., Lionello, R., & Antiochos, S. K. 2011, *ApJ*, 731, 111
- Titov, V. S., Mikic, Z., Török, T., Linker, J. A., & Panasenco, O. 2012, *ApJ*, 759, 70
- Török, T., Aulanier, G., Schmieder, B., Reeves, K. K., & Golub, L. 2009, *ApJ*, 704, 485
- Torrence, C. & Compo, G. P. 1998, *Bulletin of the American Meteorological Society*, 79, 61
- Wang, H. & Liu, C. 2012, *ApJ*, 760, 101
- Wang, Y. M., Sheeley, Jr., N. R., & Rich, N. B. 2007, *ApJ*, 658, 1340
- Wyper, P. F., Antiochos, S. K., & DeVore, C. R. 2017, *Nature*, 544, 452
- Wyper, P. F., DeVore, C. R., & Antiochos, S. K. 2018, *ApJ*, 852, 98
- Wyper, P. F., Lynch, B. J., DeVore, C. R., et al. 2024, *ApJ*, 975, 168
- Xue, Z., Yan, X., Cheng, X., et al. 2016, *Nature Communications*, 7, 11837
- Yan, X., Xue, Z., Jiang, C., et al. 2022, *Nature Communications*, 13, 640
- Yang, J., Hong, J., Li, H., & Jiang, Y. 2020a, *ApJ*, 900, 158
- Yang, L., Xue, Z., Wang, J., et al. 2024a, *ApJ*, 976, 135
- Yang, L., Yan, X., Xue, Z., et al. 2024b, *MNRAS*, 528, 1094
- Yang, L., Yan, X., Zhang, J., et al. 2025, *ApJ*, 987, 193
- Yang, S., Zhang, Q., Xu, Z., et al. 2020b, *ApJ*, 898, 101
- Zhang, Q. 2024, *Reviews of Modern Plasma Physics*, 8, 7
- Zhang, Q. M., Chen, P. F., Guo, Y., Fang, C., & Ding, M. D. 2012, *ApJ*, 746, 19
- Zhang, Y., Zhang, Q., Song, D., et al. 2022, *ApJS*, 260, 19
- Zhong, Z., Guo, Y., Ding, M. D., Fang, C., & Hao, Q. 2019, *ApJ*, 871, 105
- Zhou, C., Shen, Y., Zhou, X., et al. 2021, *ApJ*, 923, 45